Observation of mode-mixing in the spatial eigenmodes of an optical microcavity

Koks, C; Exter, M.P. van

Research Article | Vol. 30, No. 2 / 17 Jan 2022 / Optics Express 700
Optics EXPRESS

Observation of mode-mixing in the spatial eigenmodes of an optical microcavity

C. KOKS* AND M. P. VAN EXTER

Huygens-Kamerlingh Onnes Laboratory, Leiden University, P.O. Box 9504, 2300 RA Leiden, The Netherlands
*koks@physics.leidenuniv.nl

Abstract: We present a method to determine the complex coupling parameter of a two-coupled-modes system by directly measuring the coupled eigenmodes rather than their eigenvalues. This method is useful because mode-mixing can be observed even if frequency shifts can not be measured. It also allows to determine the complex coupling parameter, from which we conclude that the observed coupling is mainly conservative. We observe mode-mixing in an optical microcavity, where the modes couple primarily at the mirror surface, as confirmed by AFM measurements. The presented method is general and can be applied to other systems to measure mode coupling more accurately and to determine the nature of the coupling.

1. Introduction

Coupled harmonic oscillators occur in all fields of physics, including optics. The coupling between harmonic oscillators or optical modes modifies the eigenmodes and shifts their eigenvalues. We propose and demonstrate a method to directly observe the eigenmodes in an optical microcavity. This is a sensitive method because it depends on the coupling amplitude instead of the coupling power; it thus allows one to also measure mode-mixing when it can not be measured in frequency shifts, for instance because the second coupled mode is too weak. The complex amplitude also contains a phase, which reveals the nature of the coupling.

Optical microcavities are versatile and flexible tools to enhance the interaction between light and matter [1,2]. This enhancement, which is proportional to the cavity finesse divided by the mode area, can be controlled in an open microcavity [3–7]. An open microcavity consists of two Distributed Bragg Reflectors (DBRs) with a tunable cavity length. The radius of curvature of the DBR and the cavity length determine the mode size, and thereby the light-matter interaction. Open microcavities can achieve similar Purcell factors as monolithic cavities [8,9].

Optical cavities support fundamental and higher-order transverse modes. At certain cavity lengths, some modes become frequency degenerate and hence couple [10–14]. The coupling of optical modes in analogous to two pendulums connected by a spring as depicted in Fig. 1. The modes of the pendulums hybridize and their eigenfrequencies shift. Instead of measuring this frequency shift, we directly look at the motion of the pendulums and determine the mode-mixing amplitude from their positions. The detection of the optical eigenmodes is more subtle because we measure intensities instead of electric fields.

In this paper, we report the direct observation of mode-mixing in far-field mode profiles and from this determine the complex coupling parameter. This mode coupling is measured in a close to ideal system with an (almost) rotational-symmetric cavity. The coupling is generated by a mismatch between the mode profile and mirror shape [15] and by non-paraxial effects [16,17]. The two modes that couple are identified and described by a generic model of two coupled harmonic oscillators. We find the nature of the coupling to be conservative.

#439224 https://doi.org/10.1364/OE.439224
Journal © 2022 Received 2 Aug 2021; revised 2 Dec 2021; accepted 2 Dec 2021; published 3 Jan 2022

Optics EXPRESS

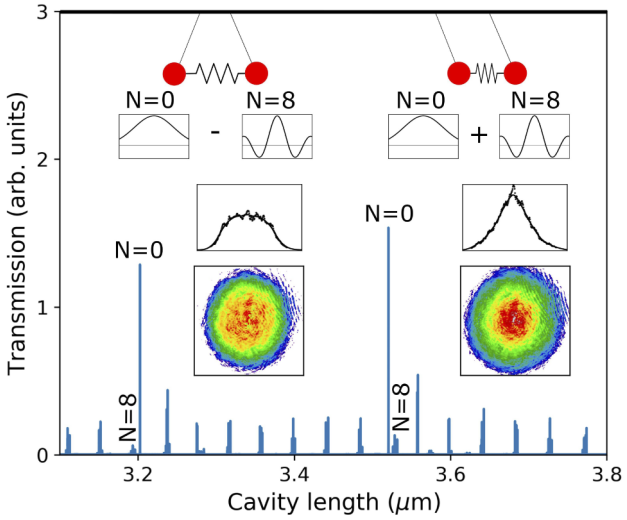

Fig. 1. Transmission spectrum around coupling of the fundamental and 8th transverse mode. The insets show CCD images of the reshaped fundamental mode together with an averaged cross-section through the center. The fundamental mode is coupled to the N=8 mode (insets only show central part), which can be in phase (right) or anti-phase (left). The $N = 8$ mode that couples has angular momentum $l = 0$ and radial mode number $p = 4$ (see below).

2. Results

Figure 1 shows a preview of our results in the form of power-normalized CCD images of two modes, close to frequency degeneracy. These images show the center intensity is increased/decreased for positive/negative coupling. A positive coupling reduces the effective mode area, theoretically up to a factor 2. Mode coupling has been proposed as a means to increase the Purcell factor [18].

The planar and concave mirrors of the microcavity are provided by Oxford HighQ and have a transmittance of $3.4(2) \times 10^{-5}$ and $1.1(1) \times 10^{-4}$ at the wavelength $\lambda = 633$ nm, close to the central wavelength of the DBR. The concave structures were fabricated with a focused ion beam [5] to produce craters with a radius $R \approx 24$ μm and an indentation depth $D \approx 0.6$ μm.

The mirrors are aligned to be parallel and almost in contact with each other. The mirror distance is scanned over a total range of 15 μm using slip-stick motors and piezo stacks. A HeNe laser ($\lambda = 633$ nm) is focused into the cavity with an $f = 8$ mm lens. The light transmitted through the cavity is collected with another $f = 8$ mm lens to measure the transmission spectrum and angular mode profiles.

Figure 1 shows the transmission spectrum with sharp high-finesse peaks at particular cavity lengths. These lengths are determined by the resonance condition, given below. The fundamental modes, indicated by $N = 0$ in Fig. 1, are also measured with a CCD camera. We use the angular mode profiles of the fundamental modes to demonstrate the mode coupling.

The paraxial eigenmodes in a rotational-symmetric cavity are Laguerre-Gaussian modes ψ_{pl}, labeled by their radial mode number p and azimuthal mode number l [19]. The transverse mode number $N = 2p + |l|$ and longitudinal mode number q determine the resonant cavity lengths L via the resonance condition $kL = q\pi + (N + 1)\chi$, with wavevector $k = 2\pi/\lambda$. The Gouy phase $\chi = \sin^{-1}(\sqrt{(L + 2L_D)/R})$, with modal penetration depth L_D [20], quantifies the phase lag of the modes with respect to a plane wave. The theoretically predicted opening angle of the fundamental mode is $\theta_0 = \lambda/(\pi w_0)$, with mode waist w_0 and Rayleigh range $z_0 = w_0^2 k/2 = R\sin(2\chi)/2$.

Optics EXPRESS

Figure 2(a) shows the measured transverse mode splitting as a function of cavity length. We plot the difference in resonant cavity length ΔL between the fundamental ($N = 0$) and the N^{th} order mode to find the Gouy phase using the relation $\Delta L/(\lambda/2) = N\chi/\pi$. A fit of the data from the $N = 1 - 5$ modes yields a radius $R = 23.8(2)$ μm and modal penetration depth $L_D = 0.03(2)$ μm. The first visible longitudinal mode is $q = 3$ because the smallest cavity length is at least as large as the indentation depth $D = 0.64(3)$ μm. The higher-order transverse modes are easier to observe in short than in long cavities, where they suffer from clipping loss. And the modes that we do observe are typically the high ℓ modes, which experience less clipping loss. We could not observe the more interesting $\ell = 0, p = N/2$ modes around the frequency degenerate points to demonstrate the expected avoided crossings with the fundamental ($N = 0$) mode (see below).

Figure 2(b) shows the opening angles θ_0 of the fundamental modes. Each point in the graph corresponds to a Gaussian fit of a CCD image. The mode profile is obtained by imaging the far-field, rather than the near-field, and is hence less sensitive to imaging aberration.

The general trend of the Gaussian fits in Fig. 2(b) follows the theoretical prediction (green curve), which is based on the parameters extracted from 2(a) and contains no fit parameters. The measured opening angle, however, strongly deviates from theory around three cavity lengths, indicated by black vertical lines in Figs. 2(ab). At these cavity lengths, the mode profile deviates from a Gaussian and exhibits features of mode-mixing. This occurs when the even transverse modes $N = 8, 6, 4$ cross the line $\Delta L/(\lambda/2) = 1$ (see Fig. 2(a)) and hence become frequency degenerate with the fundamental mode. The dominant mixing with even modes suggests a rotational-symmetric coupling effect. The modest deviation at the point indicated by $q = 25$ also indicates some mixing with $N = 5$ modes, but this mixing is significantly smaller. Modest deviations are also observed for points at the beginning, where the mode waist is somewhat smaller. The effective radius of curvature is larger for these small modes, as confirmed by atomic force microscopy (AFM) measurements (see Supplement 1).

Figure 3 explains how the mode mixing in Fig. 2(c) is quantified. Two angular mode profiles are shown, which are observed at cavity lengths corresponding to $q = 18$ and $q = 19$. These profiles show rings at larger angles, which indicates that a Gaussian fit with only the fundamental mode ψ_{00} no longer suffices and a two-mode fit is required to determine the contribution of the higher-order mode [14]. The $l = 0$ mode dominates the mixing, due to the rotational symmetry of the cavity, such that $N = 2p$ for the coupled modes. For the two-mode fit, we use the amplitude profile $\psi = (\alpha\psi_{00} + (-1)^p\beta\psi_{p0})$, with a complex mixing ratio $c_{p0} = \beta/\alpha$ and real-valued field-profiles ψ_{00} and ψ_{p0}. The phase lag between the fundamental and the higher-order mode from the near-field to the far-field is incorporated in the factor $(-1)^p$, such that the amplitude of the coupling constant relates directly to the field profiles at the flat mirror. If c_{p0} is positive and real-valued, the central part of the fields interfere constructively at the flat mirror and destructively at the curved mirror.

We first fit with complex mixing ratios c_{p0}. These fits shows that the real part of c_{p0} can be accurately fitted and varies a lot around the frequency degenerate points, whereas the imaginary part is far less accurate and more or less constant at a value between 0.2 and 0.3 (see Supplement 1). The latter value might seem significant, but the mode profile only changes with the square of imaginary part, so only 5% of power is affected by this effect. From this observation, we conclude that the mode-mixing is mainly determined by the real part of c_{p0}. Next, we fit the intensity profiles in Fig. 2(c) with a real-valued mixing-ratio c_{p0}. The fit for the points $q = 18$ and 19 are shown in Fig. 3. The two-mode fit $|\psi_{00} - c_{30}\psi_{30}|^2$ yields mixing ratios $c_{30} = -0.72(5)$ and 0.17(1) for modes $q = 18$ and 19, respectively. These values are close to the values $\text{Re}(c_{30}) = -0.58(6)$ and 0.19(1) that we obtained for the full complex fits.

Figure 2(c) shows the mixing ratio c_{p0} for all cavity lengths. To obtain these data, we fit all CCD images with two-mode fits rather than Gaussian fits. The theoretical opening angle θ_0 from Fig. 2(b) is used to describe the uncoupled modes. Three regions in Fig. 2(c) are identified in

Optics EXPRESS

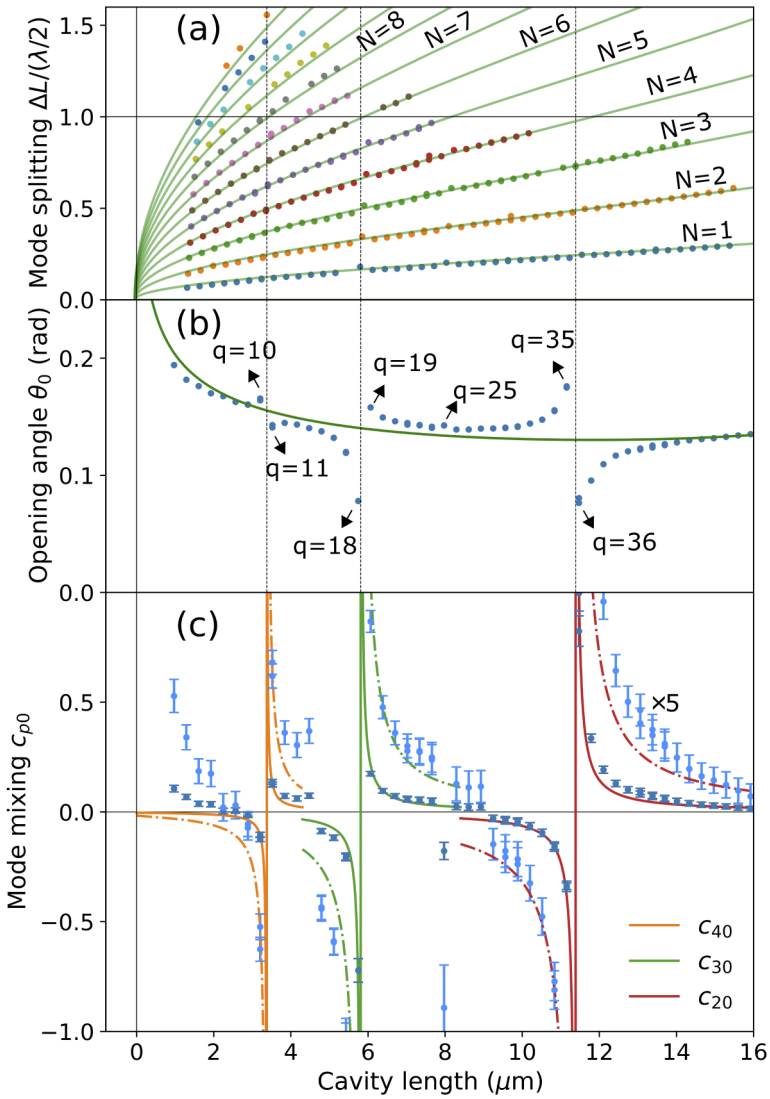

Fig. 2. (a) Transverse mode splitting versus mirror position for all visible transverse modes. (b) The Gaussian opening angle θ_0 of the fundamental mode obtained from CCD images. The green line shows the theory for the uncoupled system. (c) Mode-mixing ratio c_{p0} of modes $p = 4, 3$, and 2 into the fundamental mode. The light-blue points show the same data points on a vertical scale that is 5× enlarged.

which the fundamental mode ψ_{00} couples either with ψ_{40}, ψ_{30} or ψ_{20}. Substantial mode-mixing is observed around the frequency degenerate points. The mode-mixing with ψ_{40} ($N = 8$) shown in Fig. 1 is slightly weaker than the mixing with ψ_{30} shown in Fig. 3. The mixing with ψ_{20} ($N = 4$) around 11.3 μm shows signatures of more than 2 modes mixing in the CCD images (figure not shown).

Coupled cavity modes behave like coupled harmonic oscillators (see Supplement 1). Two modes, continuously excited by an input field through a mirror with transmission t, reach an

Optics EXPRESS

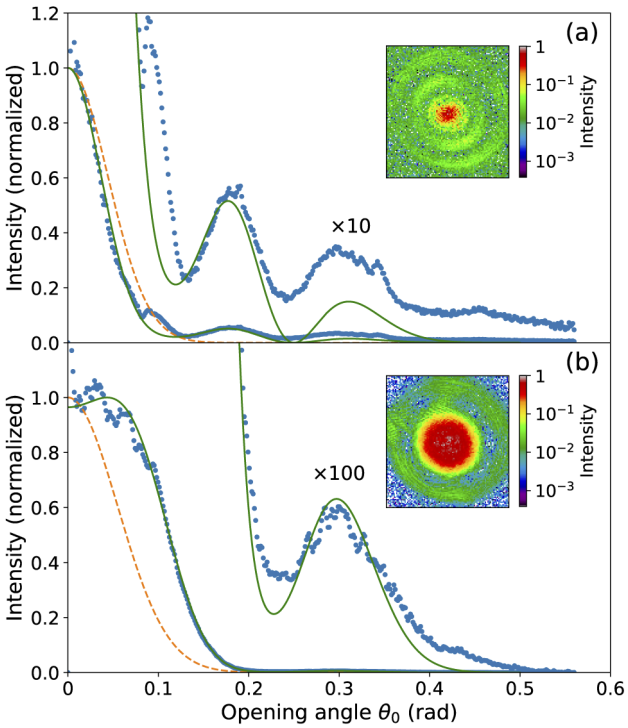

Fig. 3. Rotation-averaged intensity of angular mode profile for (a) q=18 and (b) q=19. The dots show the experimental results from the 2D intensity profiles shown as insets. The orange dashed curves show the uncoupled Gaussian shapes. The smooth green curves show the fitted two-mode shapes with fit parameters (a) $c_{30} = -0.72(5)$ and (b) $c_{30} = 0.17(1)$

equilibrium described by

$$\begin{pmatrix} i(\varphi_a - \varphi) + \gamma_a & -M_{ab} \\ -M_{ba} & i(\varphi_b - \varphi) + \gamma_b \end{pmatrix} \begin{pmatrix} \alpha \\ \beta \end{pmatrix}_c = t \begin{pmatrix} \alpha \\ \beta \end{pmatrix}_{in} \tag{1}$$

where the parameters in the matrix are dimensionless and describe variations per roundtrip. The roundtrip phase of a plane wave is given by $\varphi = 2kL$, and the roundtrip phase of the N^{th} transverse eigenmode is $\varphi_{a/b} = 2\pi q + 2(N+1)\chi(L)$. Note that each uncoupled mode is resonant if $\varphi = \varphi_{a/b}$. The roundtrip losses $\gamma_{a/b}$ determine the finesse of the uncoupled modes via $F = \pi/\gamma$.

The two modes couple at the concave mirror, where a mismatch between the mirror shape and the wavefront causes light to scatter from mode ψ_a into mode ψ_b and vice versa. This coupling is quantified by a dimensionless coupling parameter $M_{ab} = \langle \psi_a 2ik\Delta z \psi_b \rangle$. The mirror-mode mismatch Δz has two contributions. First, it contains the deviations of the mirror from a paraboloid. Second, it contains non-paraxial effects, which cause the wavefront to deviate from a paraboloid (see Supplement 1). The first contribution is dominant in our microcavities.

The coupled-harmonic-oscillator model is used to fit the data in Fig. 2(c). The solution to Eq. (1) predicts a mixing ratio $c_{ab} = \frac{M_{ba}}{i\Delta\varphi + \gamma_{ab}}$ for small enough coupling parameters (see Supplement 1). In our measurement, the detuning $\Delta\varphi = \varphi_b - \varphi_a$ is typically much larger than $\gamma_{ab} = \gamma_b - \gamma_a$, so that the latter can safely be neglected. A fit of the observed mixing ratios $c_{p0}(\Delta\varphi)$ in the three regions gives $M_{40} = 0.018(3)i$, $M_{30} = 0.031(4)i$ and $M_{20} = 0.029(2)i$.

The coupled-mode model also predicts a shift in resonance frequencies, so one expects to see avoided crossings around the frequency degenerate points in Fig. 2(a). We have not been able to

Optics EXPRESS

quantify this effect in a reliable manner for two reasons. First and most important, the finesse of the higher-order mode drops rapidly due to clipping losses for larger cavity length towards and beyond the frequency degenerate point. Furthermore, the input beam is matched better to the fundamental mode than to higher-order modes. As a result, we could not directly observe the higher-order $\ell = 0, N = 2p$ modes around the mode crossing and could only observe their mixing effect on the fundamental mode.

All three values of M_{p0} are purely imaginary with a positive imaginary part. This is experimentally evidenced by the strong interference effects in Fig. 3, which correspond to real-valued mixing ratios c_{ab}. The coupling must hence be due to a wavefront mismatch at the curved mirror, and not due to clipping losses at the edges of the mirror. The positive sign for all three couplings suggests that the wavefront mismatch dominantly occurs at the center of the curved mirror (see Supplement 1).

To find the precise origin of the coupling, we have measured the shape of the concave mirror with AFM imaging. We find a rotational-symmetric defect, which elevates the central part of the concave mirror by 0.08(2) μm with respect to the ideal parabolic shape with radius of curvature $R = 23.8$ μm (see Supplement 1). The coupling parameters M_{p0} calculated from this mirror height profile are $M_{40} = 0.015i$, $M_{30} = 0.049i$ and $M_{20} = 0.042i$. The coupling M_{40} agrees reasonably well with the optical data, but the AFM-based estimations of M_{30} and M_{20} are a factor 1.4 larger than the optical measurements. This discrepancy can partially be assigned to a non-paraxial correction, which reduces the calculated mode coupling for $p = 2$ by $\Delta M_{20} \approx 0.004i$, and to optically transparent height defects on the micromirror which only shown up in AFM measurements.

Measurements on different cavities have shown the same mode-coupling effects (see Supplement 1). The magnitude of the coupling is similar to that of the cavity presented here. Also the sign is similar, which suggests that the effect that causes the coupling is similar. This shows that the effect is general and occurs in different systems.

3. Conclusion

In summary, we have accurately measured the intensity profiles and opening angles of the fundamental mode in a microcavity as a function of cavity length. The general trend is as expected, but strong deviations were observed around three cavity lengths, where the fundamental mode couples with different higher-order modes. The coupling is conservative and is attributed to a mismatch between the mirror shape and the wavefront. The measured mode-mixing ratios near the frequency-degenerate points are substantial. This can potentially reduce the mode area and increase the Purcell factor, theoretically up to a factor 2 [18].

Rather than measuring an avoided crossing in the frequency spectrum, we observe the mode coupling directly in the far-field mode profile. This is a sensitive and powerful method, which directly yields the complex mixing ratio c_{ab} from which the complex coupling parameter M_{ab} is derived. We have not been able to measure frequency shifts or dips in finesse from mode coupling. But we have been able to measure mode coupling in the far-field mode profiles, since that effect scales linearly instead of quadratically with the coupling parameter. The amplitude and phase of the coupling parameter provide information about the nature of the coupling.

Acknowledgments. We like to acknowledge M.J.A. de Dood and X. Chen for fruitful scientific discussions and help with preparing the manuscript.

Disclosures. The authors declare no conflicts of interest.

Data availability. Data underlying the results presented in this paper are not publicly available at this time but may be obtained from the authors upon reasonable request.

Supplemental document. See Supplement 1 for supporting content.

Optics EXPRESS

References

1. K. J. Vahala, "Optical microcavities," Nature **424**(6950), 839–846 (2003).
2. I. Fushman, D. Englund, A. Faraon, N. Stoltz, P. Petroff, and J. Vučković, "Controlled phase shifts with a single quantum dot," Science **320**(5877), 769–772 (2008).
3. R. J. Barbour, P. A. Dalgarno, A. Curran, K. M. Nowak, H. J. Baker, D. R. Hall, N. G. Stoltz, P. M. Petroff, and R. J. Warburton, "A tunable microcavity," J. Appl. Phys. **110**(5), 053107 (2011).
4. L. Greuter, S. Starosielec, D. Najer, A. Ludwig, L. Duempelmann, D. Rohner, and R. J. Warburton, "A small mode volume tunable microcavity: Development and characterization," Appl. Phys. Lett. **105**(12), 121105 (2014).
5. A. A. P. Trichet, P. R. Dolan, D. M. Coles, G. M. Hughes, and J. M. Smith, "Topographic control of open-access microcavities at the nanometer scale," Opt. Express **23**(13), 17205 (2015).
6. C. A. Potts, A. Melnyk, H. Ramp, M. H. Bitarafan, D. Vick, L. J. LeBlanc, J. P. Davis, and R. G. DeCorby, "Tunable open-access microcavities for on-chip cavity quantum electrodynamics," Appl. Phys. Lett. **108**(4), 041103 (2016).
7. G. Wachter, S. Kuhn, S. Minniberger, C. Salter, P. Asenbaum, J. Millen, M. Schneider, J. Schalko, U. Schmid, A. Felgner, D. Hüser, M. Arndt, and M. Trupke, "Silicon microcavity arrays with open access and a finesse of half a million," Light: Sci. Appl. **8**(1), 37 (2019).
8. D. Najer, I. Söllner, P. Sekatski, V. Dolique, M. C. Löbl, D. Riedel, R. Schott, S. Starosielec, S. R. Valentin, A. D. Wieck, N. Sangouard, A. Ludwig, and R. J. Warburton, "A gated quantum dot strongly coupled to an optical microcavity," Nature **575**(7784), 622–627 (2019).
9. D. Wang, H. Kelkar, D. Martin-Cano, D. Rattenbacher, A. Shkarin, T. Utikal, S. Götzinger, and V. Sandoghdar, "Turning a molecule into a coherent two-level quantum system," Nat. Phys. **15**(5), 483–489 (2019).
10. T. Klaassen, J. de Jong, M. van Exter, and J. P. Woerdman, "Transverse mode coupling in an optical resonator," Opt. Lett. **30**(15), 1959–1961 (2005).
11. J. Benedikter, T. Hümmer, M. Mader, B. Schlederer, J. Reichel, T. W. Hansch, and D. Hunger, "Transverse-mode coupling and diffraction loss in tunable Fabry-Pé rot microcavities," New J. Phys. **17**(5), 053051 (2015).
12. J. Benedikter, T. Moosmayer, M. Mader, T. Hümmer, and D. Hunger, "Transverse-mode coupling effects in scanning cavity microscopy," New J. Phys. **21**(10), 103029 (2019).
13. A. A. Trichet, P. R. Dolan, and J. M. Smith, "Strong coupling between 0D and 2D modes in optical open microcavities," J. Opt. **20**(3), 035402 (2018).
14. A. T. Papageorge, A. J. Kollár, and B. L. Lev, "Coupling to modes of a near-confocal optical resonator using a digital light modulator," Opt. Express **24**(11), 11447–11457 (2016).
15. D. Kleckner, W. T. Irvine, S. S. Oemrawsingh, and D. Bouwmeester, "Diffraction-limited high-finesse optical cavities," Phys. Rev. A **81**(4), 043814 (2010).
16. K.-M. Luk, "Improvement in the resonant formula of a spherical Fabry–Perot resonator with unequal mirrors," J. Opt. Soc. Am. A **3**(1), 3 (1986).
17. C. W. Erickson, "High order modes in a spherical fabry-perot resonator," IEEE Trans. Microwave Theory Tech. **23**(2), 218–223 (1975).
18. N. Podoliak, H. Takahashi, M. Keller, and P. Horak, "Harnessing the mode mixing in optical fiber-tip cavities," J. Phys. B: At., Mol. Opt. Phys. **50**(8), 085503 (2017).
19. A. E. Siegman, *Lasers* (University Science Books, Mill Valley, California, 1986).
20. C. Koks and M. P. van Exter, "Microcavity resonance condition, quality factor, and mode volume are determined by different penetration depths," Opt. Express **29**(5), 6879–6889 (2021).